

Background model of Phoswich X-ray detector on board small balloon

Abhijit Roy, Ritabrata Sarkar*, Sandip K. Chakrabarti

Indian Centre for Space Physics, 43 Chalantika, Garia Station Road, Kolkata 700084, W.B., India

Abstract

We performed a detailed modelling of the background counts observed in a phoswich scintillator X-ray detector at balloon altitude, used for astronomical observations, on board small scientific balloon. We used Monte Carlo simulation technique in Geant4 simulation environment, to estimate the detector background from various plausible sources. High energy particles and radiation generated from the interaction of Galactic Cosmic Rays with the atmospheric nuclei is a major source of background counts (under normal solar condition) for such detectors. However, cosmogenic or induced radioactivity in the detector materials due to the interaction of high energy particles and natural radioactive contamination present in the detector can also contribute substantially to the detector background. We considered detailed 3D modelling of the earth's atmosphere and magnetosphere to calculate the radiation environment at the balloon altitude and deployed a proper mass model of the detector to calculate the background counts in it. The calculation satisfactorily explains the observed background in the detector at 30 km altitude (atmospheric depth: 11.5 g/cm^2) during the balloon flight experiment from a location near 14.5°N geomagnetic latitude.

Keywords: Scintillation detectors, Cosmic-ray interactions, Background radiations

*Corresponding author:

Email addresses: `ritabrata.s@gmail.com` (Ritabrata Sarkar), `aviatphysics@gmail.com` (Ritabrata Sarkar), `sandipchakrabarti9@gmail.com` (Sandip K. Chakrabarti)

1. Introduction

Astrophysical observations in X-ray or γ -ray energy band are carried out via space-borne or balloon-borne platforms to avoid the absorption of these rays in the earth's atmosphere. Proper understanding of the background in X-ray or γ -ray detectors used in this purpose is very important; since the detectors work in a condition of low signal-to-noise ratio, due to low intensity radiation from the distant astronomical sources as received at Earth. This knowledge is particularly necessary to reduce the background counts in the detector by optimizing its design and also to extract the source signal effectively from the observed data. The source of radiation background of space-borne or balloon-borne detectors are physically the same, but the local radiation intensity and spectra vary due to various space-weather phenomena such as: radiation belts, South Atlantic Anomaly, solar energetic particles, cosmic radiation modified by the heliospheric electromagnetic-field varying with solar activity, atmospheric residual and albedo radiation etc. The detector background strongly depends on the local space radiation environment, which changes with the position and time of observation. For example, at balloon altitude, the radiation belt and the South Atlantic Anomaly will have nominal effects, while the atmospheric residual and albedo radiations will give a substantial contribution to the detector background.

The near-earth space radiation mainly composed of Galactic Cosmic Ray (GCR) and Solar Particles Events (SPEs). The GCR consists of highly ionizing proton ($\sim 89\%$), alpha ($\sim 10\%$), small fraction of heavier nuclei and electrons, which continuously bombard on the earth's atmosphere. The primary GCR at the top of our atmosphere undergoes modulation due to heliospheric electromagnetic-wind and geomagnetic-field effect before entering the earth's atmosphere. The GCR particles then interact with the atmospheric nuclei to generate a cascade of secondary particles and radiation, which in turn creates a typical radiation intensity profile in the atmosphere. On the other hand, SPEs

are originated from the sun via coronal mass ejection and/or solar flares, which can last from a few hours to a few days. The particles from SPEs are usually less energetic than primary GCR and may extend up to a few GeVs during strong solar activity.

The background count of an X-ray detector used in astronomical observations, on board a balloon-borne platform, suffers most from these varying atmospheric secondary radiations. The total background in the detector can be considered to be due to integrated contributions from: (i) direct energy depositions from the aforementioned energetic particles and radiation in the active detector; (ii) locally produced secondary particles and radiation generated via interaction with the passive materials present in the vicinity of the active detector; (iii) radioactive decay of the cosmogenic radio-nuclides produced in the detector due to spallation and activation of the nuclei of the detector materials by the highly energetic Cosmic Ray (CR) particles; (iv) radiation from the decay of natural radio-isotopes present in the detector and its surrounding materials (Dean et al., 1991). It is worth mentioning another contribution to the balloon-borne detector background from the terrestrial radioactivity. But this component is prevalent only up to 2-3 km ($\sim 750\text{-}670\text{ g/cm}^2$) from the Earth's surface (see Fig. 2a) and diminish rapidly due to atmospheric absorption.

The Monte Carlo (MC) simulation technique is an efficient method to accurately model the detector background and has been extensively used for this purpose. However, simulation of the radio-activated background component is quite complicated task which has been successfully implemented, for example, by Weidenspointner et al. (2005) and Odaka et al. (2018), to explain the observed background of satellite-borne X-ray detectors. For heavily shielded, ground based, low background, dark matter probing experiments the observed counts have also been explained by considering the radio-activation along with the natural radioactive background of the detector and its surrounding material by several authors (Adhikari et al., 2017, 2018; Abdelhameed et al., 2019).

Here, in this work, we use a similar kind of methodology to explain the observed background of a balloon-borne X-ray detector using extensive MC

simulation with Geant4 simulation toolkit (Agostinelli et al., 2003).

The scientific ballooning team in Indian Centre for Space Physics, Kolkata, India, has been involved in small balloon-borne experiments to observe the extraterrestrial radiation for the past several years (Chakrabarti et al., 2017, and references therein). Because of the imposed payload weight constraint, the detectors used in these experiments can neither use heavy shielding nor any pointing devices. This affects the observational results in terms of poor reduction of the physical background. This constraint also does not permits us for simultaneous measurement of background during the observations of astronomical radiation sources. Furthermore, the detector undergoes diverse radiation environment during its operation as it ascends gradually towards the burst altitude of the balloon and while coming down thereafter. So, an accurate background modeling is a necessity for extracting any meaningful results out of our observed data. We have been mostly relying on the empirical solutions for the background estimation of the detectors (Sarkar et al., 2019, 2020). Here in this work, we successfully explain the total observed detector background by considering the sources of all plausible major background components through extensive MC simulation.

In Sec. 2, first we briefly describe the experimental observation considered in this work to study the background counts. Then we discuss the simulation methodology to model the detector background in Sec. 3. We show the results of the background modelling and its comparison with the observed counts in Sec. 4 and conclude the results in Sec. 5.

2. Experimental Overview

We have been using small and light-weight X-ray detectors on board small sized (~ 4000 cubic meters) plastic-balloon platform for the observation of astronomical sources in X-ray energy band. The balloon carries the payload of about 5 kg weight, up to $\sim 40\text{--}42$ km ($\sim 2.9\text{--}2.2$ g/cm²) above the earth's surface where the residual atmosphere is small enough to allow incoming X-rays

from the extraterrestrial sources. Usually, there is no cruising level for this kind of balloon flights as there are no ballast and valve system used in these carriers. The balloon goes up, get ruptured at certain level due to excess internal pressure and gradually comes down with the payload with an average speed of about 4 m/s (may vary drastically, particularly during descent, depending on the nature of rupture of the balloon) (Chakrabarti et al., 2017). The main X-ray detection unit, used in the experiment under consideration, is a scintillator detector consisting two crystals (3 mm thick NaI(Tl) and 25 mm thick CsI(Na), both of 116 mm diameter) in phoswich combination and optically coupled with a Photo-Multiplier Tube (PMT). We use a collimator, made of 0.5 mm thick tantalum providing 15° Field-of-View (FoV), to minimize the off axis radiation. In this study, we consider only the events with its full energy deposited in the primary (NaI) crystal to discard the background counts due to partial energy depositions. This has been achieved by considering the anticoincidence technique using the pulse shape information of the events recorded by the detector readout system. The pulse shape information dictates whether the signal is from the NaI crystal or have energy depositions in both the crystals (or may be in CsI crystal alone).

The background count of the detector provides a minimum detection limit above which any astronomical source could be detected. The sensitivity calculation of the detector shows that the residual atmosphere allows the detector to observe typical astronomical X-ray sources (like Crab pulsar) above the altitude of 30 km (11.5 g/cm^2) (Sarkar et al., 2020). Here, in this work, we use the results of the mission *Dignity 113* which was launched from Muluk, West Bengal, India (latitude: 23.64°N ; longitude: 87.71°E ; geomagnetic latitude: 14.5°N) on November 23, 2019 at 05:41 UT. Further information of the experiment could be found in Table 1. The operating energy range of the detector is $\sim 10\text{--}100$ keV. However, for the present analysis, we have considered only $\sim 10\text{--}80$ keV range to avoid the computational complications due to the collimator transparency at higher energy range.

Table 1: Experimental overview

Main detector	phoswich detector having 3 mm NaI crystal and 25 mm CsI crystal
Collimator	0.5 mm thick Ta collimator with 15° FoV
Other ancillary instruments	GPS system, payload tracker system, attitude measurement system
Total payload weight	5.610 kg
Detector orientation	towards local zenith
Payload carrier	one meteorological plastic balloon (length: ~ 25 m, weight: 8.075 kg)
Date of launch	Nov 23, 2019
Time duration	05:41 – 13:33 UT
Launching location	Muluk, WB, India (Lat: 23.64°N, Lon: 87.71°E)
Maximum height attains	40.09 km (at 07:50 UT)
Landing location	Bali Number 2, WB, India (Lat: 22.81° N, Lon: 87.77° E)

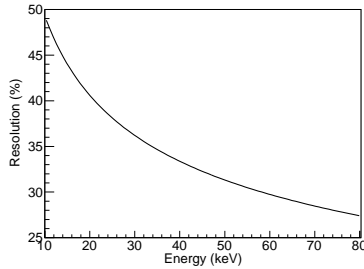


Figure 1: Energy resolution of the detector as a function of energy.

2.1. Detector calibration and resolution

During the mission preparation phase, the detector is thoroughly tested under different experimental conditions (temperature/pressure) in the laboratory. The energy calibration of the detector is done using standard calibration radiation sources (^{133}Ba , ^{137}Cs , ^{152}Eu and ^{241}Am) to find the energy-channel relation. The energy resolution of the detector is obtained by Gaussian fitting of the decay peaks of the calibration sources. (The energy resolution being defined as full-width at half-maximum divided by the mean energy of the Gaussian peaks.) The energy dependence of the resolution was found to vary as $1.944((E + 0.226)/0.083)^{-0.285}$ (E being the energy in keV) and is graphically shown in Fig. 1. The detailed procedure and results of the extensive laboratory testing can be found in Bhowmick et al. (2019). The detector resolution is necessary for the spectral analysis of the detector data, as well as to compare the simulated and observed results.

2.2. Observational data

The detector data is recorded and stored, on board in a memory-card provided to the payload, throughout the mission life from launching to landing. The observed radiation count rate, averaged over 1 minute time bin, is shown in Fig. 2a, along with the instantaneous payload altitude starting from the balloon launch. The peak in the atmospheric radiation count at about 16 km ($\sim 104 \text{ g/cm}^2$) is due to the Regener-Pfotzer maximum and has been discussed in more

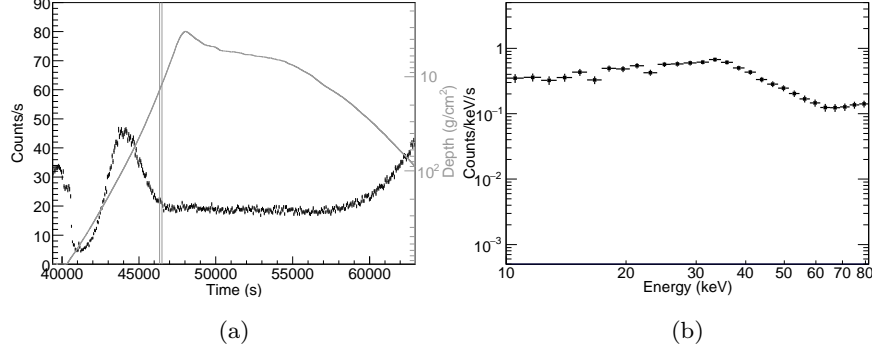


Figure 2: (a) Integrated atmospheric radiation count rate in the 10-80 keV energy range detected by the phoswich detector during the entire mission flight (black points), along with the payload altitude profile (gray line). Vertical lines showing the region around 30 km from where the detector data is considered for background analysis. (b) The background spectrum of the detector at 30 km altitude.

details in Sarkar et al. (2017). Due to some unresolved instrumental problem, the detector ceased to operate at around 17 km ($\sim 88 \text{ g/cm}^2$) altitude during the payload descent. However, the data obtained from the rest of the mission is adequate for the purpose of the current work. We consider the radiation spectrum due to atmospheric background counts at 30 km ($\sim 11.5 \text{ g/cm}^2$) altitude (marked by vertical lines in Fig. 2a). Figure 2b shows the detector spectrum (total count rate) due to the overall radiation at 30 km.

3. Simulation of Detector Background

3.1. Simulation methodology

For the simulation of background counts in a detector on board a balloon-borne platform, we mainly need to consider the following points: the radiation environment surrounding the detector, a proper mass model of the detector and its surrounding materials and the physics processes which dictates the interactions of the radiation or particles with the detector. To take account of the total observed background counts in the detector, we need to simulate background

counts due to: (i) instantaneous energy depositions in the detector from the high energy particles and radiation (along with those produced in the materials close by the detector); (ii) the prompt and delayed radioactive decay of cosmogenic induced radionuclides produced in the detector due to activation and spallation of nuclei in the detector materials by the high-energy particles and (iii) decay of long-lived natural radioactive isotopes present in the detector materials (Peterson, 1975).

First of all, we simulate the background counts from direct energy depositions of atmospheric secondary CR particles in the detector considering: a proper mass model of the detector, radiation environment and physical interaction model. Calculation of the radiation environment model of the detector, at the position of interest, is done by considering detailed atmospheric and magnetospheric models. We considered the NRLMSISE-00 standard atmospheric model (Picone et al., 2002) to describe the earth’s atmosphere up to 100 km from the earth’s surface with proper input parameters for location, time and solar condition. The inner magnetic field at the vicinity of the earth’s surface due to earth’s magnetism is calculated using the 12th generation IGRF model (Thébault et al., 2015). The external magnetic field which depends on the interplanetary magnetic field and solar condition is calculated using Tsyganenko model (Tsyganenko & Andreeva, 2016). The detailed procedure of this simulation can be found in Sarkar et al. (2020). Considering the location and time (at quiet solar condition) of the experiment, we use only the GCR spectrum with proper model (Vos & Potgieter, 2015; Herbst et al., 2017), as the primary input in the simulation without any SPE contribution. The spectral and directional distribution of the produced secondary particles and radiation at the relevant atmospheric location are used for further calculation of the background counts through simulation of radiation interaction in the detector.

To account the background due to cosmogenic radio-activation, we calculate the production of radio-nuclides in the detector via activation or spallation process, for each simulation event (i.e., incident particle). The production of cosmogenic radioactive isotopes, after the irradiation of detector mass model

are calculated using the *G4RadioactiveDecay* process provided in the Geant4 toolkit. Whenever any cosmogenic radionuclide is produced, we record the information of their mass number (A), atomic number (Z), excitation energy (ExEng), kinetic energy, position, momentum and pdg encoding (MC particle numbering scheme according to Particle Data Group (2020)). Furthermore, to avoid the double counting in the energy deposition, we kill the track of that radionuclide and all its subsequent tracks. After recording all the cosmogenic radio-nuclides from the irradiation of all the GCR interactions, we separately simulate these induced radioactive nuclei allowing them to decay in proper decay channel(s), considering their position, momentum and excitation energy in the detector materials. One caveat is worth mentioning here, if the cosmogenic radionuclides (parent) induced in the active crystal by the GCR, decays within the characteristic signal decay time of the crystal itself, the whole energy deposition from the direct interaction and radioactive decay will provide a single event signal. Although, in principle, this effect should be taken into consideration during digitization of the simulated event, in the current procedure we have not considered this effect. Practically, in the current procedure this does not affect the result substantially, since in this analysis we found no significant abundance of induced parent radio-isotopes which promptly decays to give rise this pile-up effect. This can be seen from the half lives of the enlisted parent isotopes in Table 3 which give the major contributions in our energy range of interest. However, the pile-up effect during energy depositions from different decay stages of the subsequent decay of induced parent isotopes has been considered inherently in the simulation, if the tracks have energy depositions in the active crystal within its signal decay time.

The internal background component of the detector due to natural radioactive isotopes in the detector material is calculated by generating the radionuclides randomly inside and on the surface of the primary crystal (NaI) of the detector and allow them to decay according to their proper decay channel(s), following the same approach as mentioned by Adhikari et al. (2017, 2018).

3.1.1. Particle generation model

During the ascent and descent of the balloon in the atmosphere, the detector undergo irradiation from diverse radiation environment as can be seen from the radiation intensity profile in Fig. 2a. So, an accurate modelling of radiation environment due to the interaction of CR particles and radiation with the atmosphere at the payload altitude under interest is necessary. For this purpose, the flux distribution of major atmospheric secondary GCR particles along with the residual primaries at that altitude are calculated according to the simulation procedure described in Sarkar et al. (2020). The simulation procedure considers all the updated atmospheric, geomagnetic field models and primary GCR flux model to propagate and transport the GCR and cosmic diffuse gamma-ray background photons (Ajello et al., 2008; Weidenspointner, 1999) into the atmosphere, considering proper modulation of the charged particles by the magnetosphere. The calculated flux distribution of major species of residual primary and secondary CR particles generated at 30 km altitude in the earth's atmosphere is shown in Fig. 3 separately for downward and upward particles. The directional distribution of the particles were calculated as a function of the cosine of zenith angle ($\cos\theta_Z$) and were fitted using (2nd or 3rd degree) polynomial functions of $\cos\theta_Z$ for different particles. For the simulation of radiation interaction in the detector considered in this work, we irradiated the detector with 10^6 particles of each species for both downward and upward particles (from two hemispherical surfaces), according to the particle flux distributions given in Fig. 3, with kinetic energy ranging from 10 keV to 800 GeV. We conserved the directional distribution of both the downward and upward particles obtained from the previous simulation of secondary particle generation, during the irradiation of the detector. The directional distribution is achieved by biasing the random distribution of the source positions on the two hemispheres according to the $\cos\theta_Z$ dependent polynomial functions from the previous step of the simulation. The direction of the particles generated at each points on the source surface are also random in cosine distribution w.r.t. the surface normal at that position. Con-

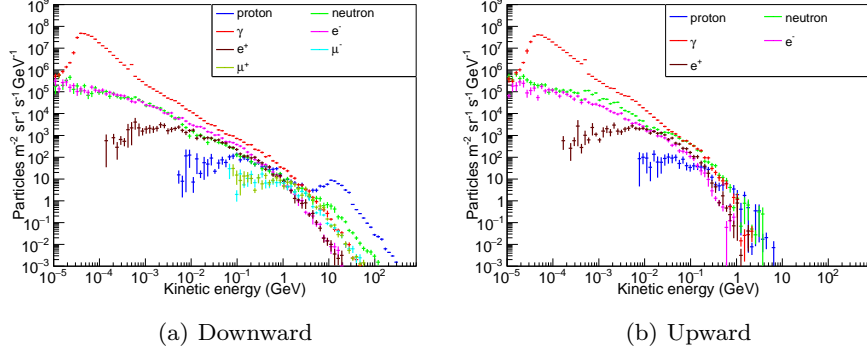


Figure 3: Flux distribution of different secondary CR (and residual primary) particles at 30 km altitude in the geomagnetic latitude range of $11.5^\circ - 17.2^\circ$, for both downward and upward particles with respect to local zenith.

sidering the geometry of the source distribution and position of the detector, we resitricted the angular random distribution in 15 deg from the surface normal direction at the position of generation, to increase the probability of the tracks hitting the detector.

3.1.2. Detector mass model

Modelling the proper mass distribution of the detector and its surrounding materials is very important, as the interaction of the high energy particles and radiation depends on this material distribution which, in turn, produce other secondary particles and induced radio-nuclides contributing to the background counts. The payload box used in the experiment is made by Styrofoam and there is no significant amount of high density materials used around the detector, apart from the thin aluminum frame to hold various payload components and PCBs for the electronic circuits (Bhowmick et al., 2019). So, here in this simulation we only consider the mass model of the detector (with PMT) along with the collimator and shielding materials. The mathematical mass model of the phoswich detector is constructed in the Geant4 simulation environment, using the realistic dimension and composition of the detector. The cut-away view

in YZ-plane of the detector mass model used in the simulation can be seen from Fig. 4.

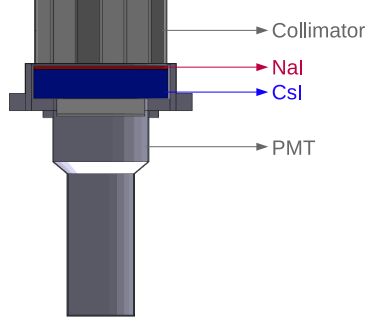


Figure 4: Cut-away view in YZ-plane of the phoswich detector module considered in the simulation.

3.1.3. Physical interaction model

Considering the requirements of the current simulation, we use *QGSP-BIC-AllHP* with updated *TALYS-based Evaluated Nuclear Data Library (TENDL)* among the many physics lists available in Geant4. This physics list is capable of handling the hadronic interactions and production of radio-nuclides which is very important for this kind of simulation. *QGSP-BIC-AllHP* is identical to *QGSP-BIC-HP* physics list except for the low energy charged particles interactions (Geant4, 2020). For electromagnetic interactions, *electromagnetic_options3* is used which is capable of handling the interactions well in the range of detection limits of the current experiment. The *QGSP-BIC-AllHP* physics list can handle hadronic interactions up to the energy of 10 TeV and the electromagnetic physics list covers the energy range from 0 to 100 TeV which is well within our required simulation range. For proper decay of radionuclide within the Geant4 toolkit, the *RadioactiveDecay5.3* and *PhotonEvaporation5.3* data sets are used. We considered the production cut value of 1 μm for gamma, electron, positron and proton during the secondary track generation in the simulation.

3.2. Signal digitization and flux normalization

NaI is the primary crystal of the scintillator detector used here for the radiation count. Any considerable energy deposition (low-level discriminator voltage is set to give trigger threshold energy around 10 keV) gives rise to a signal in the detector. However, a relatively thick CsI crystal is placed just beneath the primary crystal to eliminate the Compton background and partial energy depositions in the primary crystal. We implemented the anticoincidence technique also in the signal digitization routine of the simulated energy depositions, just as is done during the analysis of the observed data.

In order to compare the simulated background with the observed background during the experiment, we need to modulate the simulated energy deposition considering the detector resolution during the signal digitization. The deposited energy inside the NaI crystal is modified according to the detector resolution shown in Fig. 1, to convert them into channel energy of the actual detector.

The normalization of the energy spectra in the detector from the direct energy depositions of CR particles is done as follows. The normalization factor is calculated by integrating the incident particle spectra over the energy range divided by the number of simulated events. Then, multiplied by the integrated area of event generation surface (i.e., area of each hemisphere) and the solid angle integrated over the domain considered in the simulation (integration of azimuthal angle over 2π and polar angle up to 15° considering cosine distribution). Thus we get the unit same as the observed count rate of the detector.

The normalization factor of the detector counts is achieved by integration over the source surface (i.e., area of the hemisphere) and the solid angle domain considered in the simulation (integration of ϕ over 2π and θ up to 15° considering cosine distribution).

The situation is different for the calculation of normalized background counts due to energy depositions from the cosmogenic induced radioactivity in the detector. Here, we modify the simulated energy deposition from the decay of radioactive isotopes using the detector resolution as usual. But the normalization of the counts can not be done by simply considering the incident particle

spectra in the same way as was done for direct energy depositions. Due to the diverse radiation-environment history witnessed by the detector during its flight, it becomes very complicated to exactly calculate the normalization factor for the background counts from the induced radioactivity. So, we consider the following procedure to calculate the normalized contribution from the induced radioactivity. The effective background due to induced radioactivity depends on their production rate due to the radiation flux incident on the detector at each layer in the atmosphere and subsequent decay of these radionuclides. This can be a complicated process to calculate. Instead, we consider a simplified assumption of fixed incident radiation flux at the height of current calculation (30 km) shown in Fig. 3, to produce the initial list of parent radioisotopes by irradiating the detector with these radiation flux. Then, these induced radioisotopes are decayed according to their respective decay channel(s) and half lives and deposited energy is calculated in the detector crystal to give background counts as mentioned in Sec. 3.1. However, we use only those radionuclides which deposit the energy in our region of interest ($\sim 10\text{-}80$ keV). The deposited energy of each individual radioisotopes are then modified according to the detector resolution. Then, all these relevant energy deposition peaks in the energy range of interest are fitted with the observed data with independent normalizations (also considering other background contributions) to get the corresponding normalization factors of the individual peaks from different induced radio-isotopes. (See Fig. 6 and 8 and discussions in Sec. 4.1.2).

In case of background counts from the long-lived natural radioactive isotopes in the detector crystal, the problem of normalization factor persists due to the unknown fraction of radioactive contamination, which mainly occurs during the crystal growth. Also, because of the poor resolution of the detector, radiation lines from the characteristics decay peaks cannot be segregated and estimated which is possible with the cryogenic solid state detectors. So, we need to rely on the calculation of the normalization factor from the fitting of calculated flux (along with other background components) with the observed data.

4. Results and Discussions

4.1. Contributions from different background sources

We now discuss the background contributions in the detector from different sources as mentioned earlier. The different energetic particles from the atmospheric radiation environment including the residual primary particles interact with the detector material distribution (considered in Sec. 3.1.2) to deposit their energy directly in the detector crystal or via production of induced radionuclides. These induced radionuclides (along with natural radioactive isotopes present in the crystal) subsequently decay according to their allowed decay channel(s) with corresponding half lives and deposit energy in the crystal. Since the observation is done at low geomagnetic region where the rigidity cut-off is high and there is no considerable solar event at the time of observation, we neglect the contribution of solar cosmic-rays to the background counts.

4.1.1. Contribution from direct energy deposition of secondary cosmic rays

Simulated flux distribution in the detector due to the major components of secondary CR particles in the atmosphere are shown in Fig. 5a. Whereas, in Fig. 5b, we show the count-rate distribution in the detector due to contributions from all the individual particle and radiation species along with the total observed count rate in the detector. We also tabulate the simulated count rates and corresponding relative contributions to the total observed background in Table 2. From these simulation results, it is quite evident that atmospheric γ -ray is the principal contributor to the total observed detector background among all the secondary GCRs, and it is quite justified because of the use of thin NaI crystal and anticoincidence technique for background reduction. Due to their energy deposition nature, most of the other particles (than γ -rays and neutrons) with lower energies will be absorbed in the materials covering the detector crystals, while the higher energy particles are likely to deposit their partial energy both in NaI and CsI crystals, thus being removed from the background counts by anticoincidence requirement. From Fig. 5b, it is also apparent that direct

Table 2: Simulated count rates (Counts/s) from different atmospheric particles and their relative contribution (Rel. Cont.) to the total observed count rate

Particle	Counts/s	Rel. Cont. (%)
p	0.028	0.126
n	0.178	0.787
γ	8.552	37.76
e^-	0.151	0.666
e^+	0.054	0.241
μ^-	0.000	0.004
μ^+	0.001	0.007

energy depositions from atmospheric CRs contribute only a part of the detector background and we need to include the background counts from other sources as well.

4.1.2. Contribution from induced cosmogenic radio-activation

The detector counts from direct energy deposition of atmospheric CR alone can not explain the observed background. Therefore, we need to consider the contribution to the background counts from the radionuclides induced in the detector through Cosmogenic Radio-Activation (CRA). For this calculation, we considered the decay simulation of all the individual cosmogenic isotopes produced through the primary plus secondary GCR interactions inside the detector. Although, a lot of different radio-nuclides are produced inside the detector, all of them do not contribute to the detector counts within the observed energy range and observation time slot. The contribution from the CRA component is calculated by considering the decay of all the radionuclides produced in the NaI crystal as described previously in Sec. 3.1 and 3.2, then find their relative contributions from their relative abundance and half lives. The normalized contribution of the cosmogenic radio-nuclides are calculated by fitting the total observed background with the simulated decay peaks, leaving only the normal-

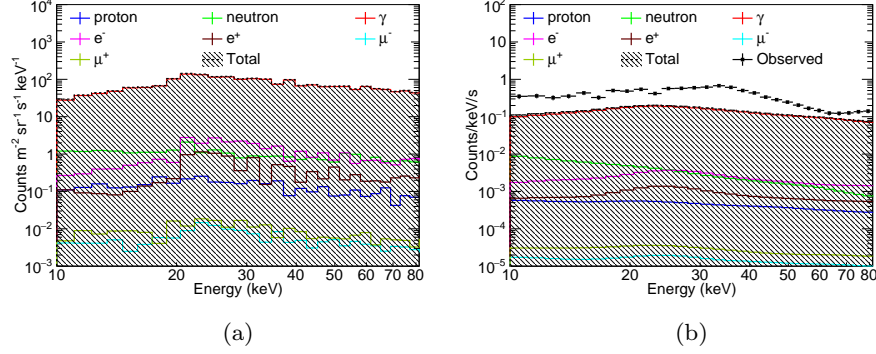


Figure 5: (a) Simulated particle flux in the detector due to different secondary CR particles in NaI crystal, with considering anticoincidence technique. (b) Contribution of different CR particles to the detector counts along with the observed detector counts at 30 km altitude.

ization parameter to float in the fitting procedure as described in Sec. 3.2. The major contributions from different cosmogenic isotopes are given in Table 3. Considering the detector resolution factor we rearranged the different isotopic contribution at similar peak energies into subgroups as shown in the table. The relative contributions of individual radio-nuclides within different subgroups are also given at the last column of Table 3 (separated with braces). These contributions from the induced radio-nuclides in comparison with the observed data can be seen from Fig. 6. Here, the count rates and relative contributions from different (sub-grouped) peaks in Table 3 are calculated from the normalization factors obtained from the fitting procedure. The contributions from different induced isotopes inside a subgroups given at the last column of the table are calculated from relative abundances of the produced isotopes and their corresponding decay rates depending on the half lives. Therefore, we can distinguish the primary contributions in each subgroup.

The major contribution to the background near 36 keV (grp1) is due to the pile-up energy deposition from the electron shell rearrangement photons following the Electron Capture (EC) process in ^{123}I . Another contribution to this energy is from EC in ^{125}I producing ^{125m}Te [35.5 keV] which stabilize to

the ground state by emitting a γ -ray (35.5 keV). A negligible amount of ^{125m}Te [144.7 keV] also produced from direct activation which subsequently decay by γ emission. ^{119}Sb decay by emitting a γ -ray around 25 keV (23.8 keV) following the EC process. All the isotopes in grp2 contributes to the background mainly by the X-ray emission due to electron shell rearrangement after EC process. ^{89}Zr also contributes near 17 keV by the same process. The contribution from ^{118m}Sb [50.8 keV] near 79 keV is due to pile-up of γ emission during transition from the metastable state and X-ray emission from atomic shell electron transition. Finally, ^{113m}Sn [77.3 keV] contributes near 79 keV by emitting a γ -ray (77.3 keV) during its transition from metastable state. Although, in Table 3 we mention the energy value only for the major contribution from each activated isotopes, there may be contributions at other energies as well, as evident from Fig. 6.

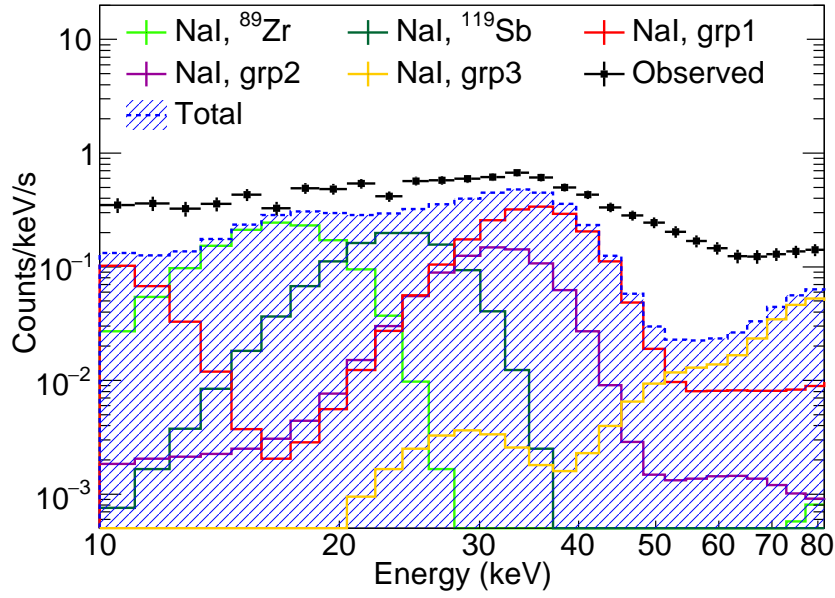


Figure 6: Contributions from different CR induced radio-activated background counts inside the NaI crystal and in the tantalum collimator along with the observed detector counts at 30 km altitude. Isotope elements contributing in grp1, grp2 and grp3 are given in Table 3.

Table 3: Simulated count rates (Counts/s) from different cosmogenic radio-activated isotopes and their relative contribution (Rel. Cont.) to the observed counts rate. Major energy deposition peaks from radioactive decay process (E_{dep}) and half life ($t_{1/2}$) of the isotopes are also given. Smaller contributions have been divided in three subgroups. Relative contributions of each radio-nuclides in their corresponding groups is given in the last column separated by braces.

Isotopes	A	Z	E_{dep}^* (keV)	$t_{1/2}$	Counts/s	Rel. Cont. (%)
^{123}I	123	53	35.9	13.22 hour	[grp1] 4.33	19.12 { 97.31
^{125}I	125	53	35.9	59.40 days		
^{125m}Te	125	52	35.9	57.40 days		
^{122}I	122	53	31.2	03.63 min	[grp2] 2.64	11.66 { 38.58
^{118}Sb	118	51	29.0	03.60 min		
^{128}I	128	53	31.2	24.99 min		
^{120}Sb	120	51	29.0	15.89 min		
^{116}Sb	116	51	29.0	15.80 min		
^{112}In	112	49	27.0	14.88 min		
^{115}Sb	115	51	29.0	32.10 min		
^{117}Sb	117	51	29.0	02.80 hour		
^{89}Zr	89	40	16.7	78.41 hour	1.95	8.62
^{119}Sb	119	51	25.0	38.19 hour	1.92	8.49
^{118m}Sb	118	51	79.3	20.6 μsec	[grp3] 1.14	5.03 { 94.08
^{113m}Sn	113	50	79.3	21.4 min		

* E_{dep} does not refer to the actual deposited energy due to the decay emission, but the bin center of the detector spectral binning in which the energy deposition contributes.

4.1.3. Contribution from internal natural radioactivity

The background contributions from the direct energy deposition of CR particles and from the induced radioactivity due to high energy CR particles are not yet able to explain the observed background completely. The missing counts near 40–50 keV region suggests other source of radiation in this region which could be due to the radiation counts from natural radioactive elements present in the detector crystal and other surrounding materials. The possible background source could be from the decay of ^{210}Pb contamination present in the detector crystal, which decays with half life around 22 years and has a γ -ray peak at around 46 keV, as also suggested by Adhikari et al. (2017) for the same type of crystal. Based on this understanding, we calculate the contribution from ^{210}Pb isotopes in a similar method following Adhikari et al. (2017). We consider a random spatial distribution of the ^{210}Pb isotopes inside the whole NaI crystal and on its surface and subsequently decay them. We considered the summed up energy for coincident depositions from the beta decay of ^{210}Pb and subsequent γ emission from the metastable ^{210m}Bi . Afterwards, we modify the recorded energy deposition by the detector resolution during the signal digitization. The simulation shows that the major contribution from the natural ^{210}Pb decay are coming from the crystal surface and not from the isotope distribution inside the crystal body.

As we already mentioned in Sec. 3.2, the normalized contribution of the Natural Radiogenic (NR) background component is obtained by fitting the overall observed background with all the components contributing to it (allowing the normalization parameter to float during the fitting). The total count rate from the decay of ^{210}Pb distributed at crystal surface is 2.19 Counts/s and its relative contribution is 9.67% of the total observed count rate, as obtained from the fitting. The background contribution obtained from the simulation of natural radioactive contamination in the NaI crystal in relation to the total observed background counts is shown in Fig. 7. While separate contributions from GCR and CRA are also shown in the figure.

We compared the fitting results of the NR component with the observation data at the position of minimum counts (at time ~ 42000 s in Fig. 2a) during the balloon flight, to get an idea about the limit of the NR component. The analysis shows that at this position there are still enough counts from other sources like direct energy depositions from GCR and CRA component, which makes it difficult to make any conclusive remark about the NR component, since no absolute measurement of this component has not been possible on experimental basis. The NR component obtained from the current fitting comprises only $\sim 20.91\%$ of the observed background at the position of minimum counts, compared to the 9.67% contribution to the total background at 30 km.

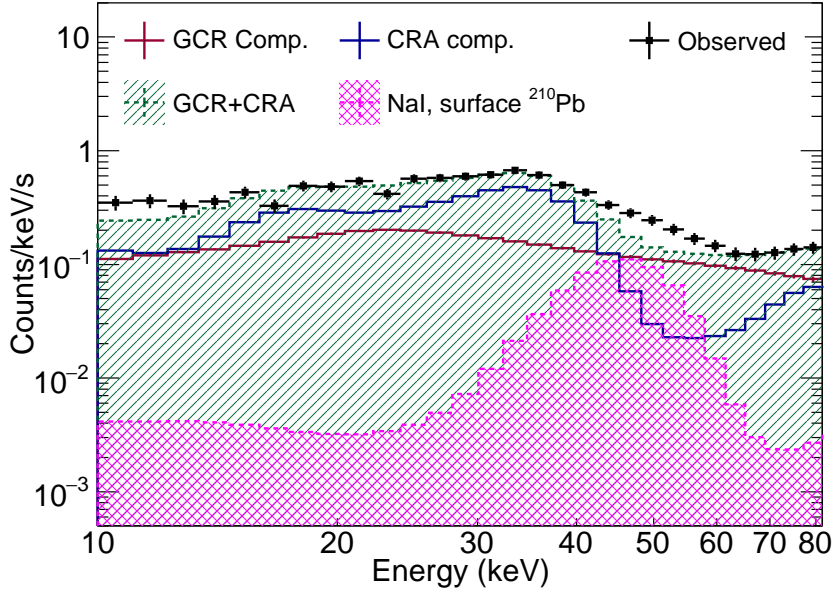


Figure 7: Contribution of natural radioactive background counts from ^{210}Pb isotopes distributed on NaI crystal surface. While GCR and CRA components are separately shown with their combined contribution.

4.2. Total background contribution

The total background calculated from the simulation consisting all the possible source of background fitted with the observed data is plotted in Fig. 8, along with the residual plot at the lower panel. All the observed data is well within the $\pm 3\sigma$ uncertainty of the simulation data. The Pearson's χ^2 test provided $\chi^2/\text{NDF} = 17.33/23$ with 0.79 as the probability factor. Thus, the overall background counts observed in the detector is explained quite satisfactorily considering the components due to energy depositions from the atmospheric CR particles, cosmogenic radio-activation and natural radioactive isotopes in the detector. Here, considering the fixed (calculated) GCR component obtained from the simulation using realistic GCR, atmospheric and geomagnetic models, the other two contributors to the detector background: CRA and NR components have been fitted with the observed data to find their unknown contribution. The GCR, CRA and NR component contributes 38.73%, 51.80% and 9.46% respectively to the total (simulated) background counts.

5. Conclusions

We have explained quite successfully the background counts from different sources and their contributions in a scintillator X-ray detector on board a small scientific-balloon platform. In general, the same procedure can be followed for other X/ γ -ray detectors on the ground or on board balloon or satellites. In this procedure, we considered the primary contribution from the GCR particles which produce other secondary particles and radiation in the atmosphere and in turn adding to the background counts in the detector. Albeit the detailed calculation of the radiation environment at balloon altitude due to these particles were done by Sarkar et al. (2020), the present calculation shows that detector background count from direct energy depositions of the particles and radiation is not enough to account for the whole background. In this work, we further extend the calculation to incorporate other effects from induced radioactivity in the detector, due to high energy CR particles by activation and spallation

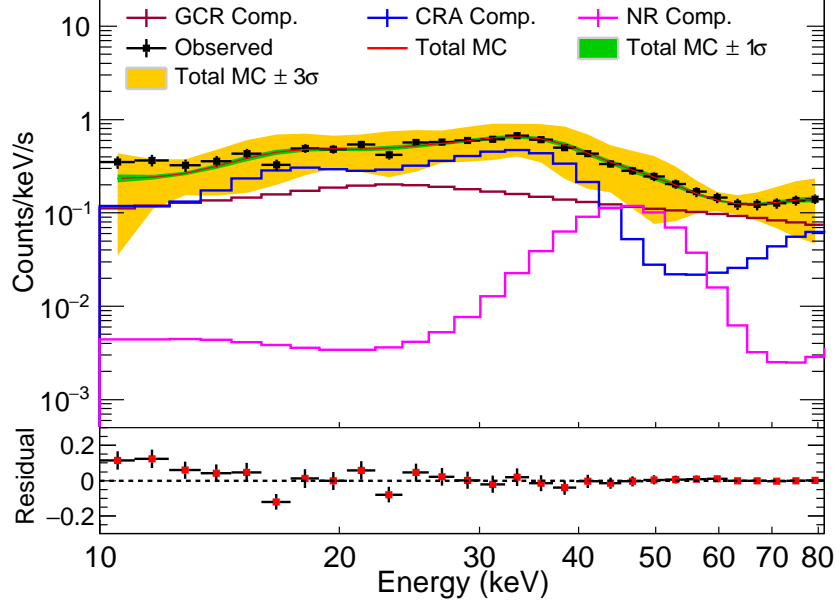


Figure 8: The observed background counts (Observed: black points) by phoswich detector at balloon altitude (30 km), along with the total simulated background spectrum (Total MC: red line) and individual contributions from different background components: Galactic Cosmic Ray component (GCR: brown histogram), Cosmogenic Radio Activation component (CRA: blue histogram) and Natural Radiogenic component (NR: pink histogram). The green and orange bands indicate the $\pm 1\sigma$ (green band) and $\pm 3\sigma$ (orange band) statistical uncertainty of the simulation calculation. The residual of the simulated and observed data is shown at the bottom panel.

of high-Z detector materials, along with the additional contribution from the natural radioactive isotopes contaminating the detector crystal. Since the experiment under consideration here was performed in a solar quiet situation, the external radiation contribution from GCR alone (along with the cosmogenic induced and natural radioactivity internal to the detector crystal) could explain the detector background counts, without considering any contribution from sun. Otherwise, it may also need to consider the SEP fluxes, in particular for the detectors on board satellites or during high solar activity. However, it is worth mentioning some note of caution regarding this calculation. The back-

ground component from the direct GCR energy depositions is dependent on the models chosen to describe the GCR spectrum, atmosphere, magnetosphere etc. So, some systematic uncertainty in this component may persist through the calculation. The contribution from other two components due to CRA and NR has been obtained by fitting the normalization factors for both of them. Though the absolute contribution from CRA is very complicated to calculate due to diverse radiation environment and history in the atmosphere, the absolute contribution from the NR component, in principle, could be obtained from an experiment considering the detector inside a well-shielded bunker or inside an active shielding box (e.g., using plastic scintillator and PMT combination and checking for anticoincident events), shunning the direct GCR and CRA contributions. However, due to some operational constraints this experiment has not been possible yet and we rely on the simulation and fitting procedure to get the relative contributions from CRA and NR components.

6. Acknowledgments

The authors would like to thank the Indian Centre for Space Physics (ICSP) scientific balloon team members, namely, Mr. D. Bhowmick, Mr. H. Roy, Mr. R. C. Das and Mr. U. Sardar for their valuable supports in various forms during the mission operations and data collection. This work been done under financial support from the Science and Engineering Research Board (SERB, Department of Science and Technology, Government of India) project No. EMR/2016/003870. We also thank the Higher Education department of West Bengal, for a Grant-In-Aid which allowed us to carry out the research activities at ICSP. All the data shown in this work are available from the authors.

References

Abdelhameed, A., Angloher, G., Bauer, P., Bento, A., Bertoldo, E., Breier, R., Bucci, C., Canonica, L., D’Addabbo, A., Di Lorenzo, S. et al. (2019).

- Geant4-based electromagnetic background model for the CRESST dark matter experiment. *The European Physical Journal C*, 79(10), 1–18.
- Adhikari, G., Adhikari, P., Ha, C., Jeon, E., Kim, N., Kim, Y., Kong, S., Lee, H., Oh, S., Park, J. et al. (2017). Understanding NaI (Tl) crystal background for dark matter searches. *The European Physical Journal C*, 77(7), 437.
- Adhikari, P., Adhikari, G., de Souza, E. B., Carlin, N., Choi, S., Choi, W., Djamal, M., Ezeribe, A., Ha, C., Hahn, I. et al. (2018). Background model for the NaI (Tl) crystals in COSINE-100. *The European Physical Journal C*, 78(6), 1–10.
- Agostinelli, S., Allison, J., Amako, K. a., Apostolakis, J., Araujo, H., Arce, P., Asai, M., Axen, D., Banerjee, S., Barrand, G. . et al. (2003). GEANT4—a simulation toolkit. *Nuclear instruments and methods in physics research section A: Accelerators, Spectrometers, Detectors and Associated Equipment*, 506(3), 250–303.
- Ajello, M., Greiner, J., Sato, G., Willis, D., Kanbach, G., Strong, A., Diehl, R., Hasinger, G., Gehrels, N., Markwardt, C. et al. (2008). Cosmic X-ray background and earth albedo spectra with Swift BAT. *The Astrophysical Journal*, 689(2), 666.
- Bhowmick, D., Chakrabarti, S. K., Sarkar, R., Bhattacharya, A., & Rao, A. R. (2019). Development of instruments for space exploration using meteorological balloons. *Journal of Astronomical Telescopes, Instruments, and Systems*, 5(3), 036001.
- Chakrabarti, S. K., Sarkar, R., Bhowmick, D., & Bhattacharya, A. (2017). Study of high energy phenomena from near space using low-cost meteorological balloons. *Experimental Astronomy*, 43(3), 311–338.
- Dean, A., Lei, F., & Knight, P. (1991). Background in space-borne low-energy γ -ray telescopes. *Space Science Reviews*, 57(1-2), 109–186.

- Geant4 (2020). Physics List Guide. <http://geant4-userdoc.web.cern.ch/geant4-userdoc/UsersGuides/PhysicsListGuide/PhysicsListGuide.html> [Online; accessed 09–August–2020].
- Herbst, K., Muscheler, R., & Heber, B. (2017). The new local interstellar spectra and their influence on the production rates of the cosmogenic radionuclides ^{10}Be and ^{14}C . *Journal of Geophysical Research: Space Physics*, 122(1), 23–34.
- Odaka, H., Asai, M., Hagino, K., Koi, T., Madejski, G., Mizuno, T., Ohno, M., Saito, S., Sato, T., Wright, D. H. et al. (2018). Modeling of proton-induced radioactivation background in hard X-ray telescopes: Geant4-based simulation and its demonstration by Hitomi’s measurement in a low Earth orbit. *Nuclear Instruments and Methods in Physics Research Section A: Accelerators, Spectrometers, Detectors and Associated Equipment*, 891, 92–105.
- Particle Data Group (2020). Monte Carlo particle numbering scheme. <https://pdg.lbl.gov/2007/reviews/montecarlopp.pdf>. [Online; accessed 09–August–2020].
- Peterson, L. E. (1975). Instrumental technique in X-ray astronomy. *Annual Review of Astronomy and Astrophysics*, 13(1), 423–509.
- Picone, J., Hedin, A., Drob, D. P., & Aikin, A. (2002). NRLMSISE-00 empirical model of the atmosphere: Statistical comparisons and scientific issues. *Journal of Geophysical Research: Space Physics*, 107(A12), SIA–15.
- Sarkar, R., Chakrabarti, S. K., Bhowmick, D., Bhattacharya, A., & Roy, A. (2019). Detection of Crab radiation with a meteorological balloon borne phoswich detector. *Experimental Astronomy*, 47(3), 345–358.
- Sarkar, R., Chakrabarti, S. K., Pal, P. S., Bhowmick, D., & Bhattacharya, A. (2017). Measurement of secondary cosmic ray intensity at Regener-Pfotzer height using low-cost weather balloons and its correlation with solar activity. *Advances in Space Research*, 60(5), 991–998.

- Sarkar, R., Roy, A., & Chakrabarti, S. K. (2020). Simulation of cosmic rays in the Earth’s atmosphere and interpretation of observed counts in an X-ray detector at balloon altitude near tropical region. *Advances in Space Research*, 65(1), 189–197.
- Thébault, E., Finlay, C. C., Beggan, C. D., Alken, P., Aubert, J., Barrois, O., Bertrand, F., Bondar, T., Boness, A., Brocco, L. et al. (2015). International geomagnetic reference field: the 12th generation. *Earth, Planets and Space*, 67(1), 79.
- Tsyganenko, N., & Andreeva, V. (2016). An empirical RBF model of the magnetosphere parameterized by interplanetary and ground-based drivers. *Journal of Geophysical Research: Space Physics*, 121(11), 10–786.
- Vos, E. E., & Potgieter, M. S. (2015). New modeling of galactic proton modulation during the minimum of solar cycle 23/24. *The Astrophysical Journal*, 815(2), 119.
- Weidenspointner, G. (1999). *The origin of the cosmic gamma-ray background in the COMPTEL energy range*. Ph.D. thesis Technische Universität München. URL: <https://mediatum.ub.tum.de/doc/602832/602832.pdf>.
- Weidenspointner, G., Harris, M., Sturmer, S., Teegarden, B., & Ferguson, C. (2005). MGGPOD: A Monte Carlo suite for modeling instrumental line and continuum backgrounds in gamma-ray astronomy. *The Astrophysical Journal Supplement Series*, 156(1), 69.